

Multi-modal 3D Pose and Shape Estimation with Computed Tomography

Mingxiao Tu; Hoijoon Jung; Alireza Moghadam; Jineel Raythatha; Lachlan Allan, Jeremy Hsu; Andre Kyme, Jinman Kim

University of Sydney
mingxiao.tu@sydney.edu.au

Abstract. In perioperative care, precise in-bed 3D patient pose and shape estimation (PSE) can be vital in optimizing patient positioning in preoperative planning, enabling accurate overlay of medical images for augmented reality-based surgical navigation, and mitigating risks of prolonged immobility during recovery. Conventional PSE methods relying on modalities such as RGB-D, infrared, or pressure maps often struggle with occlusions caused by bedding and complex patient positioning, leading to inaccurate estimation that can affect clinical outcomes. To address these challenges, we present the first multi-modal in-bed patient 3D PSE network that fuses detailed geometric features extracted from routinely acquired computed tomography (CT) scans with depth maps (mPSE-CT). mPSE-CT incorporates a shape estimation module that utilizes probabilistic correspondence alignment, a pose estimation module with a refined neural network, and a final parameters mixing module. This multi-modal network robustly reconstructs occluded body regions and enhances the accuracy of the estimated 3D human mesh model. We validated mPSE-CT using proprietary whole-body rigid phantom and volunteer datasets in clinical scenarios. mPSE-CT outperformed the best-performing prior method by 23% and 49.16% in pose and shape estimation respectively, demonstrating its potential for improving clinical outcomes in challenging perioperative environments.

Keywords: In-bed 3D Pose and Shape Estimation · Computed Tomography · Multi-modal Fusion

1 Introduction

In hospitals, perioperative care encompasses clinical support provided before (preoperative), during (intraoperative), and after (postoperative) surgery to ensure patient safety, comfort, and optimal recovery [19]. A notable portion of patients remain confined to bed during perioperative care. Approximately 15% of patients are bedridden preoperatively, and nearly 100% spend the entire surgical procedure on the operating table (typically lasting 2-6+ hours) [23]. After surgery, studies also found that 30–40% remain in bed postoperatively due to complications from a few days to weeks depending on the types of operations [10]. This extended immobility could contribute to adverse outcomes such as

pressure ulcers, affecting 2.5 million patients annually in the U.S. alone [2]. Accurate three-dimensional (3D) patient pose and body shape estimation (PSE) is defined as estimating the pose and shape of the patient, and generating a 3D parametric human mesh model from one or more input data, including RGB-D images, infrared (IR) images, or pressure maps (PM) [26,21,15]. It can model the patient body in 3D and potentially improve care at each stage of the perioperative process. For instance, in preoperative planning, precise patient PSE can guide optimal patient positioning and the adjustment of medical equipment to prevent pressure injuries [1,11]. During surgery, real-time PSE enhanced by augmented reality can overlay the patient’s medical images onto the body to provide surgeons with an ‘X-ray’ visualization for decision-making [14]. Postoperatively, continuous PSE monitoring can identify deviations from prescribed positions to promote optimal wound healing or respiratory mechanics [4,5].



Fig. 1. In-bed PSE can face occlusions and complex poses, overlaid by 3D mesh [16].

Existing in-bed patient PSE methods [26,9,8,24,7] typically rely on end-to-end deep networks and derive a widely used 3D Skinned Multi-Person Linear model (SMPL) that decouples human shape and pose into low-dimensional parameter spaces [17] (see Fig. 1). This model can represent the dynamic human body in 3D digital mesh by using 10-dimensional shape and 72-dimensional pose vectors. Clever et al. [7] presented a deep learning model that infers an SMPL model based on PM and gender. Yin et al. [26] leveraged multimodal data (RGB-D, IR, and PM) to improve in-bed PSE, and Zheng et al. [27] introduced a self-supervised framework with 2D keypoint estimations based on RGB-D images. More recently, Tandon et al. [24] proposed BodyMAP that jointly predicted the SMPL model and a 3D pressure map using depth and 2D pressure images. However, these PSE methods often struggle with various occlusions including medical drapes, missing data when body parts are not in contact with sensors, and complex in-bed patient poses, leading to less accurate SMPL estimation.

To address these limitations, we introduce **Multi-modal In-bed Patient 3D Pose and Shape Estimation with Computed Tomography (mPSE-CT)**, a new multimodal deep neural network that uses CT data and depth maps as inputs. CT data, often acquired for preoperative assessment [20], intraoperative navigation [25], or postoperative evaluation [13], provide a reliable “reference” for the patient’s body surface which can compensate for occluded information. Our

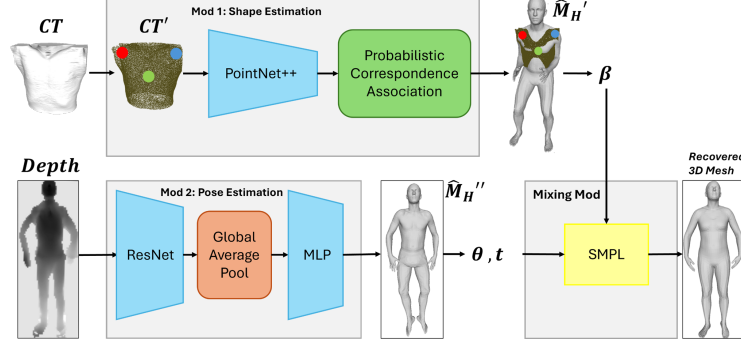


Fig. 2. mPSE-CT overview which infers 3D SMPL mesh from CT and depth map.

method effectively extracts detailed surface features from CT data through the shape estimation module, along with the pose estimation module, which derives pose from depth maps. This unique fusion not only addresses occlusion issues but also leverages detailed shape information. mPSE-CT is evaluated using two proprietary datasets: a phantom dataset (with supine and left-oriented lateral poses, with and without drapes), and a volunteer dataset (with supine and right-oriented lateral poses) in a simulated medical setting. Each data set provides the paired 3D mesh, 2D depth image, CT data and registered SMPL models. The phantom dataset is also made publicly available. The performance of mPSE-CT is compared against the state-of-the-art approaches, demonstrating its potential to improve in-bed PSE in challenging perioperative environments.

2 Methodology

Our model mPSE-CT comprises two parallel modules: body shape estimation and pose estimation; and a parameter mixing module to generate the final patient body mesh (see Fig. 2). We employ the SMPL model [17], which represents the human body shape and pose using a small set of parameters, enabling efficient 3D mesh reconstruction. It includes pose $\theta \in \mathbb{R}^{24 \times 3}$, shape $\beta \in \mathbb{R}^{10}$ parameters and global translation $t \in \mathbb{R}^3$. In SMPL, β are predefined principal component analysis shape coefficients that capture deviations from a standard T-shaped SMPL template, reflecting body measurements including torso dimensions; θ encode relative 3D joint rotations in an axis-angle format to simulate pose changes.

2.1 Body Shape Estimation Module

Given a CT image, the body shape estimation module aims to predict β . CT image is segmented to isolate the body surface and remove the CT scanner bed by applying intensity thresholding and morphological operations, and reconstructed into a 3D mesh using the marching cubes algorithm [18]. The CT

mesh is transformed into a point cloud by randomly and uniformly sampling 5,000 points (see Fig. 2 CT'). We adopt Zuo et al.'s [28] probabilistic framework as the backbone architecture to extract local and global features from the point cloud using PointNet++ [22]. Then in β optimization, the vertices of the SMPL model are treated as centroids of a Gaussian Mixture Model (GMM), and correspondences between the vertices of a template SMPL model and the point cloud are established. The probability of a point v_n in the input is modelled as:

$$p(v_n) = (1 - \mu) \sum_{m=1}^{|M|} \pi_{mn} \mathcal{N}(v_n | M_m(\Theta)) + \mu \frac{1}{N} \quad (1)$$

where π_{mn} represents the soft alignment of v_n to the template vertices of SMPL model M_m , and μ accounts for potential outliers. M , N are the number of vertices and \mathcal{N} is a normal distribution. Once the probability distribution for each point in the input is computed, the probabilistic correspondence association (PCA) module updates the posterior probability of each point corresponding to vertices on the SMPL model. The updated soft correspondences are then used to define a loss function that minimizes the discrepancy between the updated SMPL model and the input. This iterative process refines the alignment by optimizing β to accurately reflect the torso shape.

2.2 Body Pose Estimation Module

The pose estimation module employs a modified BodyMap network to exclusively process the top-viewing depth map of the in-bed patient to predict θ and t [24]. The depth map is first normalized, denoised using a median filter, and resized to (128,54) in size. Then it is encoded using ResNet18 [12], which extracts latent features, and then processed through a multi-layer perceptron (MLP) to regress θ and t . This architecture is trained using a new loss function, as defined below:

$$L = L_{SMPL} + \lambda_1 L_{v2v} + \lambda_2 L_{height} \quad (2)$$

where L_{SMPL} minimizes the error of SMPL parameters, L_{v2v} minimizes the error of mesh vertices, and L_{height} minimizes the discrepancy between the predicted body height and the known height information from the CT metadata.

2.3 Parameter Mixing Module

Finally, the parameter mixing module concatenates the estimated β from the body shape estimation module and the estimated θ and t from the pose estimation module to produce a fully parameterized SMPL model $\hat{M}_H(\beta, \theta, t)$. The CT data provides the shape parameters that are closer to true body measurements (e.g., limb length, torso length, body mass) which are independent and not space-related to pose parameters in SMPL.

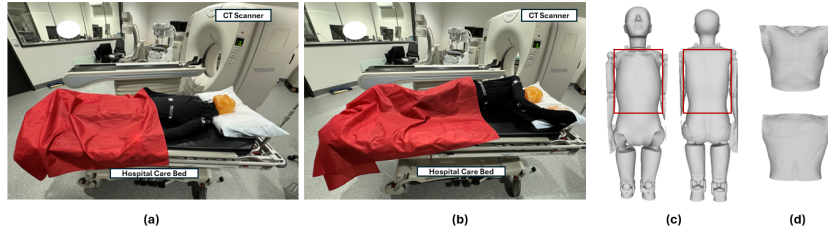


Fig. 3. Phantom is scanned in supine (a) and lateral (b). Phantom CT (c) (red rectangle is the cropped torso region used for Module 1) and volunteer CT (d) are shown.

3 Experimental Setup and Evaluation

3.1 Phantom and Volunteer Dataset

The phantom dataset was collected under four configurations using the PBU-60 whole-body phantom (Kyoto Kagaku Co.) in two poses (supine, left-lateral) and two occlusion conditions (with/without drape). CT data of the phantom were acquired with a Toshiba Alexion CT scanner in $512 \times 512 \times 1703$ voxels (spacing: $0.761 \times 0.761 \times 0.8$ mm³). To generate its top-view 2D depth map, the dressed phantom was placed on a hospital bed and scanned with a Microsoft HoloLens2 (Microsoft Corporation, Redmond, WA, USA) for a 3D surface scan (see Fig. 3(a), 3(b)). The resulting mesh was projected to a 2D depth map via a virtual rendering camera located above the phantom. Acquiring the 3D mesh first enables accurate SMPL ground truth registration for each pose acquired. Ground truth SMPL registration was obtained by aligning SMPL models to the 3D HoloLens2 meshes using an off-the-shelf algorithm [3], followed by manual refinement and projection to 2D to align with depth maps. The alignment incorporated data loss (chamfer distance between the SMPL model and the 3D scan), landmark loss (L2 distance between SMPL model landmarks and scan landmarks), prior shape loss (L2 norm of the SMPL shape parameters), and prior pose loss (GMM prior loss) to ensure a robust fit and to establish reliable GT.

Two healthy male volunteers participated with ethics approval granted by the Ethics Committee of the Western Sydney Local Health District (2021/ETH00209) (Volunteer 1 – height 172 cm; weight 77 kg; right lateral pose; Volunteer 2 – 173 cm height; weight 70 kg; supine pose; both without drapes). CT data were acquired using Vereos Digital PET/CT scanner that only captured the thorax part (see Fig. 3(d)). Top-viewing 2D depth maps and GT SMPL models were generated the same method used in the phantom dataset.

3.2 Evaluation

To evaluate 3D pose estimation performance, Mean Per-Joint Position Error (MPJPE) and Per-Vertex Error (PVE) were computed. MPJPE calculates the

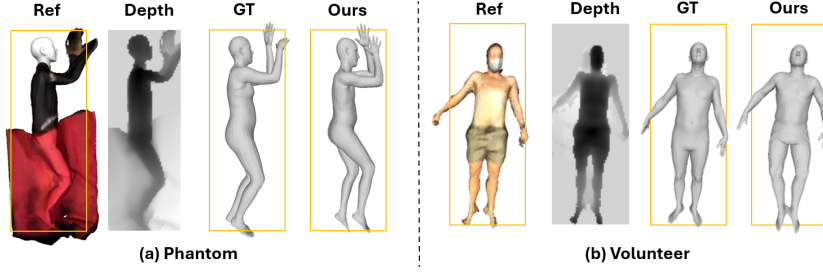


Fig. 4. SMPL prediction on selected configurations in phantom (right-oriented, covered) and volunteer (supine, no cover) datasets. The input CT is in Fig.3 (c), (d).

average Euclidean distance between the predicted 3D joint positions from the estimated SMPL model and the GT positions from the GT SMPL model. PVE calculates the average Euclidean distance between corresponding vertices of the predicted and GT SMPL models. To evaluate performance in 3D body shape estimation, anatomical accuracy was quantified by calculating the circumference of the chest, waist, and hips on the SMPL model, as proposed by Choutas et al. [6]. These shape metrics were computed as the absolute error between the predicted and the GT anatomical measurements.

To evaluate the impact of incorporating CT-derived β , we assessed vertex-to-vertex (V2V) error focusing on the torso region, which is also clinically significant due to its susceptibility to occlusions. Moreover, we conducted an ablation study where we fixed the θ and varied β derived from different modalities. We compared the following three configurations: (1) exclusive employment of CT-derived β ; (2) employment of depth map-derived β ; and (3) averaging β derived from CT data and depth map. For the baseline comparison, we selected open-source state-of-the-art in-bed PSE methods that take depth maps as the input including BPBNet [8], BPWNet [8], and BodyMap-PointNet [24]. While some prior multi-modal methods incorporate additional modalities such as PM or IR data, they were not included as baselines because our data collection was limited to depth and CT modalities.

Table 1. 3D pose and shape errors between mPSE-CT and SoTA.

Methods	3D Pose Error (mm) ↓		3D Shape Error (cm) ↓		
	MPJPE	PVE	Chest	Waist	Hip
BPBNet [8]	89.31 ± 3.01	-	-	-	-
BPWNet [8]	76.48 ± 2.45	91.20 ± 2.08	9.82 ± 0.32	19.59 ± 0.34	12.81 ± 0.42
BodyMap-PNet [24]	63.75 ± 1.83	72.98 ± 1.77	5.38 ± 0.24	4.36 ± 0.21	5.57 ± 0.21
mPSE-CT	48.91 ± 1.31	58.56 ± 1.12	2.52 ± 0.43	2.76 ± 0.18	2.36 ± 0.12

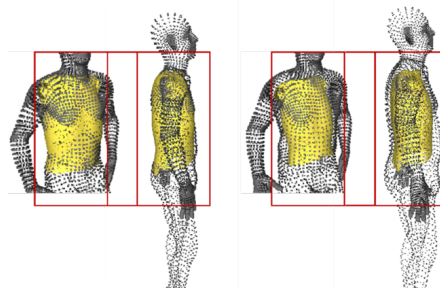


Fig. 5. SMPL prediction (black dot) from mPSE-CT (left) and the BodyMap-PointNet (right), aligning with ground truth phantom CT data (yellow mesh).

Table 2. V2V error under various configurations for phantom (P) and volunteer (V).

Conf.	V2V (cm) ↓				
	GT	BPBNet	BPWNet	BodyMap-PNet	mPSE-CT
P-Back	0.19 ± 0.17	0.26 ± 0.24	0.27 ± 0.22	0.23 ± 0.22	0.20 ± 0.19
P-Back, draped	0.23 ± 0.23	0.33 ± 0.26	0.34 ± 0.25	0.31 ± 0.23	0.25 ± 0.26
P-LSide	0.31 ± 0.18	0.41 ± 0.31	0.40 ± 0.28	0.34 ± 0.27	0.31 ± 0.22
P-LSide, draped	0.29 ± 0.25	0.38 ± 0.28	0.39 ± 0.26	0.33 ± 0.25	0.30 ± 0.26
V-Back	0.18 ± 0.16	0.25 ± 0.21	0.25 ± 0.21	0.23 ± 0.22	0.22 ± 0.19
V-RSide	0.24 ± 0.17	0.37 ± 0.28	0.36 ± 0.25	0.29 ± 0.23	0.30 ± 0.29

4 Results and Discussion

4.1 Pose and Body Shape Estimation

Table 1 summarizes the errors of mPSE-CT in estimating the patient’s in-bed pose and body shape, with averages computed over all configurations from both the phantom and volunteer datasets. mPSE-CT achieved an MPJPE of 48.91 mm for pose estimation, outperforming the best-performing state-of-the-art method BodyMap-PointNet (MPJPE: 63.75 mm) by 23%. In body shape estimation, mPSE-CT resulted in the best accuracy of 2.52 cm (chest), 2.76 cm (waist), and 2.36 cm (hip), achieving a 53.16%, 36.70% and 57.63% enhancement over BodyMap-PointNet, respectively. These improvements underscore the importance of the addition of CT data in our network compared to depth-only approaches. The qualitative results are also presented in Fig. 4. By providing accurate patient surface details, CT data enabled accurate shape estimation of a patient’s true body contours, even with occlusions. Additionally, enhanced accuracy in body shape estimation provides a better context for determining joint positions, contributing to more precise patient pose estimation.

4.2 Body Shape Estimation on Torso

Table 2 presents the accuracy of body shape estimation specifically on the torso for each configuration. In the phantom "Back" configuration, mPSE-CT achieved

a V2V error of 0.20 ± 0.19 cm, outperforming BodyMap-PointNet. Similar trends were observed in lateral configurations, with mPSE-CT yielding the lowest errors. mPSE-CT resulted in lower errors in the volunteer dataset, with 0.18 ± 0.16 cm for "Back" and 0.24 ± 0.17 cm for "Side" poses, reflecting similar advantages on real human shape variations. Notably, configurations with drapes yielded slightly higher errors, emphasizing the challenge from occlusion. The qualitative results are presented in Fig. 5 where mPSE-CT notably aligned better with the raw CT data, suggesting that it could effectively extract detailed surface data from CT and use it for the estimation.

Table 3. Averaged results for ablation study from phantom and volunteer.

Regime	MPJPE (mm) ↓	MPVPE (mm) ↓
Shape based on depth	78.34 ± 2.32	85.91 ± 2.47
Shape based on CT	48.91 ± 1.41	58.56 ± 1.35
Shape based on depth + CT	54.37 ± 1.87	64.75 ± 1.69

4.3 Ablation study

Table 3 shows the average MPJPE and MPVPE results for shape parameters derived from depth-only, CT-only and depth+CT. Employment of CT-derived β improved both 3D shape and pose estimations, achieving the lowest errors (MPJPE = 48.91 mm, MPVPE = 58.56 mm). This suggests that CT modality provides more accurate body shape measurements compared with depth maps. Additionally, better shape estimations refine joint localization and enhance overall pose accuracy. Averaging shape parameters from CT and depth still improves performance (MPJPE = 54.37 mm, MPVPE = 64.75 mm) compared to using depth alone, which yields the highest error (MPJPE = 78.34 mm, MPVPE = 85.91 mm).

5 Conclusion

We proposed mPSE-CT, a novel multi-modal network that integrates CT data and depth maps to enhance the accuracy of in-bed patient PSE. Our network effectively leverages CT data for its detailed shape information and routine use in perioperative settings, confirming the clinical feasibility of our approach. The comprehensive evaluation demonstrates that mPSE-CT achieved better results surpassing the state-of-the-art methods. These improvements translate into more precise 3D patient body models, which can guide patient positioning, enhance surgical navigation through improved augmented reality overlays, and support better postoperative monitoring. Future work includes exploring other imaging modalities' performance, including MRI and PET, in the 3D in-bed PSE task.

References

1. Berhouet, J., Samargandi, R.: Emerging innovations in preoperative planning and motion analysis in orthopedic surgery. *Diagnostics* **14**(13), 1321 (2024)
2. Berlowitz, D., VanDeusen Lukas, C., Parker, V., Niederhauser, A., Silver, J., Logan, C., Ayello, E.: Preventing pressure ulcers in hospitals: a toolkit for improving quality of care. *Agency for Healthcare Research and Quality* **1** (2011)
3. Boja, D.: Smpl-fitting. <https://github.com/DavidBoja/SMPL-Fitting> (2020), accessed: 2023-10-27
4. Casas, L., Navab, N., Demirci, S.: Patient 3d body pose estimation from pressure imaging. *International journal of computer assisted radiology and surgery* **14**, 517–524 (2019)
5. Chen, K., Gabriel, P., Alasfour, A., Gong, C., Doyle, W.K., Devinsky, O., Friedman, D., Dugan, P., Melloni, L., Thesen, T., et al.: Patient-specific pose estimation in clinical environments. *IEEE journal of translational engineering in health and medicine* **6**, 1–11 (2018)
6. Choutas, V., Müller, L., Huang, C.H.P., Tang, S., Tzionas, D., Black, M.J.: Accurate 3d body shape regression using metric and semantic attributes. In: *Proceedings of the IEEE/CVF Conference on Computer Vision and Pattern Recognition*. pp. 2718–2728 (2022)
7. Clever, H.M., Erickson, Z., Kapusta, A., Turk, G., Liu, K., Kemp, C.C.: Bodies at rest: 3d human pose and shape estimation from a pressure image using synthetic data. In: *Proceedings of the IEEE/CVF conference on computer vision and pattern recognition*. pp. 6215–6224 (2020)
8. Clever, H.M., Grady, P.L., Turk, G., Kemp, C.C.: Bodypressure-inferring body pose and contact pressure from a depth image. *IEEE Transactions on Pattern Analysis and Machine Intelligence* **45**(1), 137–153 (2022)
9. Clever, H.M., Kapusta, A., Park, D., Erickson, Z., Chitalia, Y., Kemp, C.C.: 3d human pose estimation on a configurable bed from a pressure image. In: *2018 IEEE/RSJ International Conference on Intelligent Robots and Systems (IROS)*. pp. 54–61. IEEE (2018)
10. Collins, T.C., Daley, J., Henderson, W.H., Khuri, S.F.: Risk factors for prolonged length of stay after major elective surgery. *Annals of surgery* **230**(2), 251 (1999)
11. Grimm, R., Bauer, S., Sukkau, J., Horneegger, J., Greiner, G.: Markerless estimation of patient orientation, posture and pose using range and pressure imaging: For automatic patient setup and scanner initialization in tomographic imaging. *International journal of computer assisted radiology and surgery* **7**, 921–929 (2012)
12. He, K., Zhang, X., Ren, S., Sun, J.: Deep residual learning for image recognition. In: *Proceedings of the IEEE conference on computer vision and pattern recognition*. pp. 770–778 (2016)
13. Heary, R.F., Bono, C.M., Black, M.: Thoracic pedicle screws: postoperative computerized tomography scanning assessment. *Journal of Neurosurgery: Spine* **100**(4), 325–331 (2004)
14. Jung, H., Raythatha, J., Moghadam, A., Jin, G., Mao, J., Hsu, J., Kim, J.: Ribmr—a mixed reality visualization system for rib fracture localization in surgical stabilization of rib fractures: Phantom, preclinical, and clinical studies. *Journal of Imaging Informatics in Medicine* pp. 1–15 (2024)
15. Lei, C., Li, F., Chen, X., Yang, L.: Pressure-based in-bed pose estimation methods using the skinned multi-person linear model. In: *2024 4th Asia Conference on Information Engineering (ACIE)*. pp. 74–79. IEEE (2024)

16. Liu, S., Huang, X., Fu, N., Li, C., Su, Z., Ostadabbas, S.: Simultaneously-collected multimodal lying pose dataset: Enabling in-bed human pose monitoring. *IEEE Transactions on Pattern Analysis and Machine Intelligence* **45**(1), 1106–1118 (2022)
17. Loper, M., Mahmood, N., Romero, J., Pons-Moll, G., Black, M.J.: SMPL: A skinned multi-person linear model. *ACM Trans. Graphics (Proc. SIGGRAPH Asia)* **34**(6), 248:1–248:16 (Oct 2015)
18. Lorensen, W.E., Cline, H.E.: Marching cubes: A high resolution 3d surface construction algorithm. In: *Seminal graphics: pioneering efforts that shaped the field*, pp. 347–353 (1998)
19. Meara, J.G., Leather, A.J., Hagander, L., Alkire, B.C., Alonso, N., Ameh, E.A., Bickler, S.W., Conteh, L., Dare, A.J., Davies, J., et al.: Global surgery 2030: evidence and solutions for achieving health, welfare, and economic development. *The lancet* **386**(9993), 569–624 (2015)
20. Merlo, A., Chen, K., Deo, S., Markowitz, A.: Does routine preoperative computed tomography imaging provide clinical utility in patients undergoing primary cardiac surgery? *Interactive Cardiovascular and Thoracic Surgery* **25**(4), 659–662 (2017)
21. Omran, M., Lassner, C., Pons-Moll, G., Gehler, P., Schiele, B.: Neural body fitting: Unifying deep learning and model based human pose and shape estimation. In: *2018 international conference on 3D vision (3DV)*. pp. 484–494. IEEE (2018)
22. Qi, C.R., Yi, L., Su, H., Guibas, L.J.: Pointnet++: Deep hierarchical feature learning on point sets in a metric space. *Advances in neural information processing systems* **30** (2017)
23. Safety, W.P., Organization, W.H., et al.: WHO guidelines for safe surgery 2009: safe surgery saves lives. No. WHO/IER/PSP/2008.08-1E, World Health Organization (2009)
24. Tandon, A., Goyal, A., Clever, H.M., Erickson, Z.: Bodymap-jointly predicting body mesh and 3d applied pressure map for people in bed. In: *Proceedings of the IEEE/CVF Conference on Computer Vision and Pattern Recognition*. pp. 2480–2489 (2024)
25. Uhl, E., Zausinger, S., Morhard, D., Heigl, T., Scheder, B., Rachinger, W., Schichor, C., Tonn, J.C.: Intraoperative computed tomography with integrated navigation system in a multidisciplinary operating suite. *Operative Neurosurgery* **64**(5), ons231–ons240 (2009)
26. Yin, Y., Robinson, J.P., Fu, Y.: Multimodal in-bed pose and shape estimation under the blankets. In: *Proceedings of the 30th ACM International Conference on Multimedia*. pp. 2411–2419 (2022)
27. Zheng, M., Planche, B., Gong, X., Yang, F., Chen, T., Wu, Z.: Self-supervised 3d patient modeling with multi-modal attentive fusion. In: *International Conference on Medical Image Computing and Computer-Assisted Intervention*. pp. 115–125. Springer (2022)
28. Zuo, X., Wang, S., Sun, Q., Gong, M., Cheng, L.: Self-supervised 3d human mesh recovery from noisy point clouds. *arXiv preprint arXiv:2107.07539* (2021)